EXTREME OCEANIC CYCLOGENESIS

L Dell'Osso
European Centre for Medium-Range Weather Forecasts
Shinfield Park, Reading, UK

1. INTRODUCTION

Validating results from limited area model (LAM) experiments is often problematic. In fact, LAMs are commonly used with a resolution higher than global models, and, even if a corresponding high resolution analysis is available, very seldom the routine observations are as dense as the grid of a high resolution LAM, especially over mountainous regions or over the ocean. There is a difference in the way of validating results from a LAM that is used for everyday forecasts and a LAM used for research. In the former, the validation is mainly made by verification against observation of weather parameters. In the latter, besides these parameters, the simulation of particular phenomena and their vertical structure are given more consideration.

Ad hoc observations are needed to verify these research simulations. Data from special observation periods of field experiments are extensively used. Among the most recent of them over the Atlantic-European area, it is worth mentioning the Experiment on Rapidly Intensifying Cyclones over the Atlantic (ERICA), Front '87, and experiments over orographic complexes as the Alps or the Pyrenees as ALPEX and PYREX. Other very useful observations are those gathered in and around tropical storms, as well as polar lows. In fact, they can give useful information on the effects of physical parametrizations at various scales. Sometimes an indirect way of verifying some of the results of a high resolution numerical experiment can be obtained by using them as input for other numerical models, as for instance a wave model, and verifying results of these models.

It is worth noting that field experiments are generally made to gather information on the nature, origin, and evolution of a particular phenomenon, in order to be able to deduce a physical theory of the phenomenon itself. However, despite more intense observation during the special period of the experiment, the quantity of observations is always limited in time and especially in space. This is particularly true for vertical structures that are quite often deduced from flights of airplanes, whose observations are extrapolated to the surrounding area. In these cases, results of a numerical model can be used in turn to validate particular observation and to support a theory of that phenomenon.

In this note, results of experiments with the ECMWF's LAM will be presented and compared with observations. The case of the polar low of 27 February 1984 (*Shapiro et al.*, 1987, hereafter *SFH*) will be presented in section 2, the case of the Mediterranean storm of 2-3 December 1989 (*Dell'Osso et al.*, 1992) in section 3, and the case of the ERICA IOP4 (*Neiman and Shapiro*, 1992), (*Neiman et al.*, 1992) in section 4.

2. THE 27 FEBRUARY 1984 POLAR LOW

The 500 hPa analysis of 0000 UTC 26 February,1984 shows a cold vortex located over Greenland (*SFH*'s Fig. 2). From this vortex a synoptic-scale short wave moves towards Iceland in the next 12 hours. A thermal trough associated with this short wave can be seen crossing Iceland during the 24 hours up to 0000 UTC 27 February, when the temperature northeast of Iceland drops from -25° C to -35° C. Downward vertical velocity behind the trough axis at 700 hPa and upward ahead of it, propagates eastward with the short wave. At 1000 hPa, a low in the eastern lee of Greenland starts its eastern movement into the Norwegian sea at 1200 UTC 26 February, and, 24 hours later, it is located near the coast of Norway over a region of conditionally unstable temperature lapse rate where a polar low develops. The rapid evolution of this polar low can be seen in the NOAA 7 and 8 satellite images reproduced in *SFH*'s Fig. 27. The simulation experiment with the ECMWF's limited area model was carried out over an area of 2220 km by 2220 km centred over the Norwegian sea. The domain was covered by 136 x 96 points, giving a grid-size of 20 km that corresponds approximately to a spectral truncation T666. The experiment started at 0000 UTC 26 February, and ended at 1200 UTC 27 February, 1984, one hour and forty minutes earlier than the observation reported by *Shapiro et al.* (1987). During this period of time the low moved and evolved considerably, nevertheless the comparison with observations gives an indication of the ability of the model in reproducing, not only qualitatively, the processes associated with this disturbance.

In Fig. 1a the wind field at 950 hPa shows the polar low with high wind north and south of it. The low produced by the model (Fig. 1b) is much broader than that observed (*SFH*'s Fig. 9b) and its centre is located almost 200 km too far north. However, its central sea level pressure of 982 hPa is as observed, as well as the temperature of its core at 950 hPa (Fig. 2 to be compared *SFH*'s Fig. 12), which is significant because this low is classified among the hurricane-like core type (*Reed*, 1988). Also the wind field at 950 hPa (Fig. 3) compares well with that observed at 300 m (*SFH*'s Fig. 10b). The order of magnitude of the simulated wind speed is the same, although the distribution is different. The maximum wind is in fact over the northern part of the low centre in the experiment and over the southern part in the observations. At this point it is worth mentioning that most of the flights went over the southern part of the polar low, as can be seen in *SFH*'s Fig. 8. Therefore in this situation the simulation is a source of information for the evolution of that part of the phenomenon that was not well observed. In a way one can talk of validation of the observations. In this sense the convective precipitation distribution simulated by the model (Fig. 4) was interesting information for the observers, as there was no detailed information from that region available.

The vertical cross section along the line AA' of Fig. 1b for the potential temperature and wind presents an unstable layer below 500 hPa (Fig. 5) as expected. This cross section can be compared with the observed cross section (*SHF*'s Fig. 19), the latter being less broad because, as already said, the resolution of the

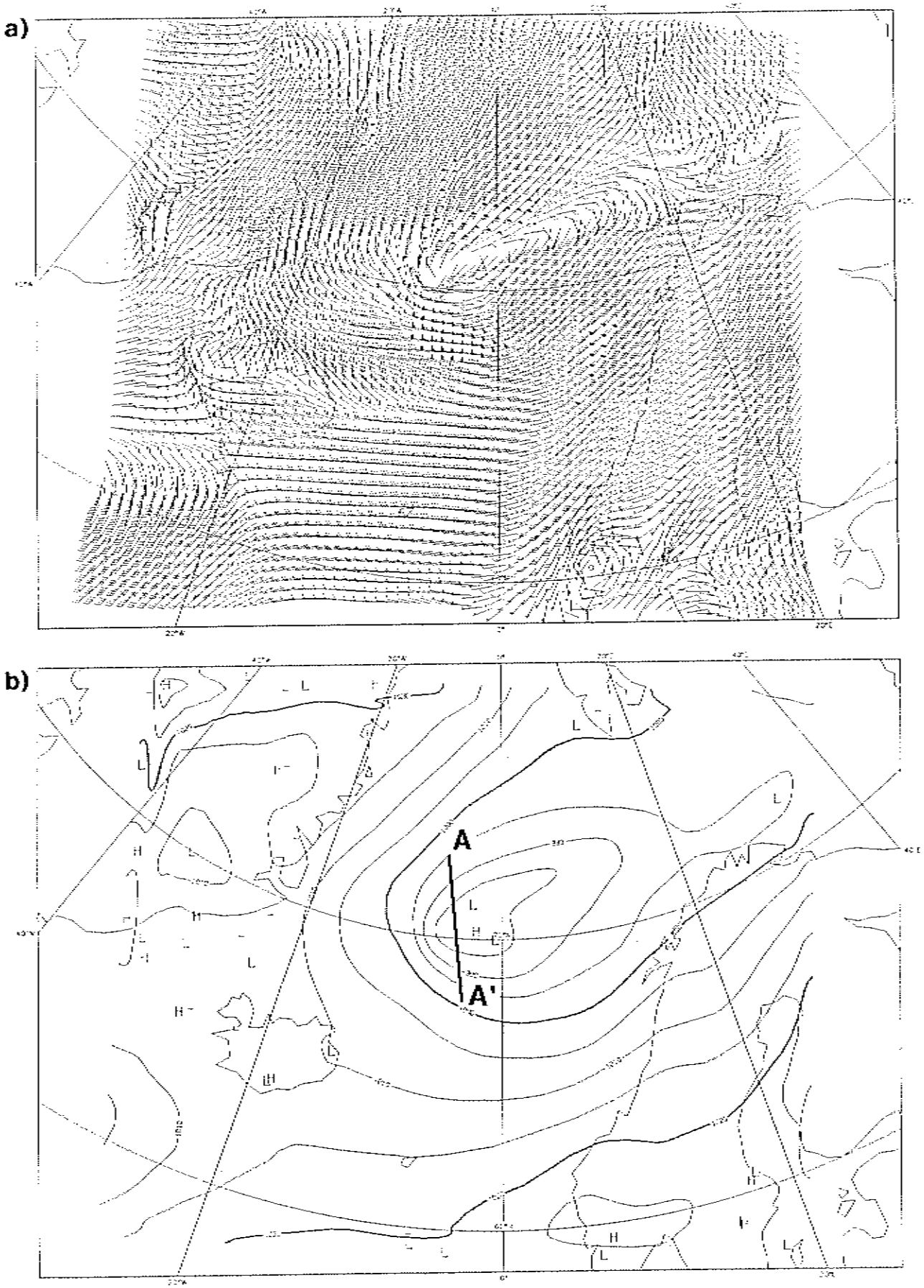

Fig.1 a) 950 hPa wind, b) mean sea level pressure at 1200 UTC 27 February, 1984.

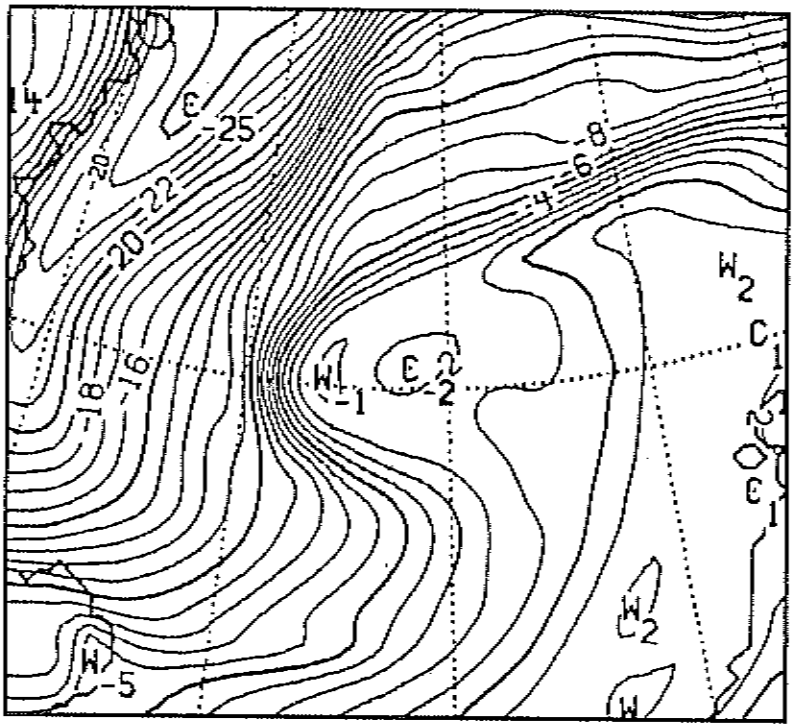

Fig.2 Simulated 950 hPa temperature (°C) at T+36h.

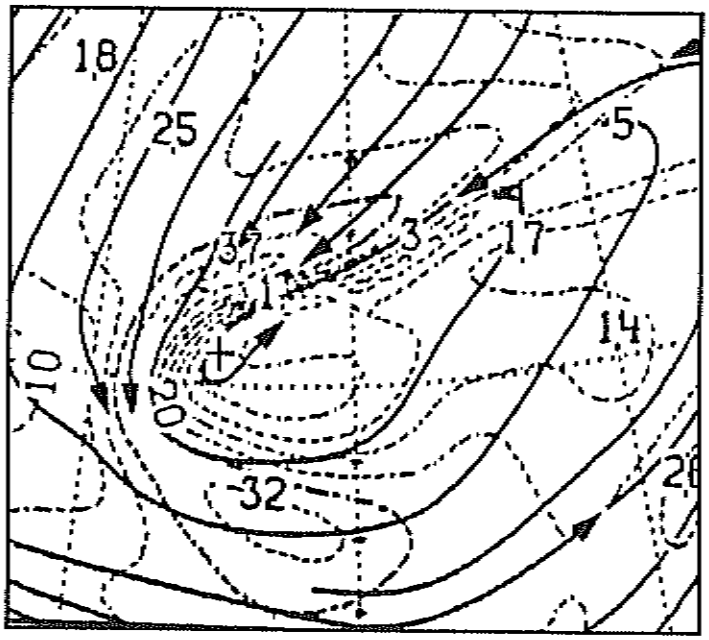

Fig.3 Simulated 950 hPa isotachs (every 5 ms^{-1}) and streamlines at T+36h.

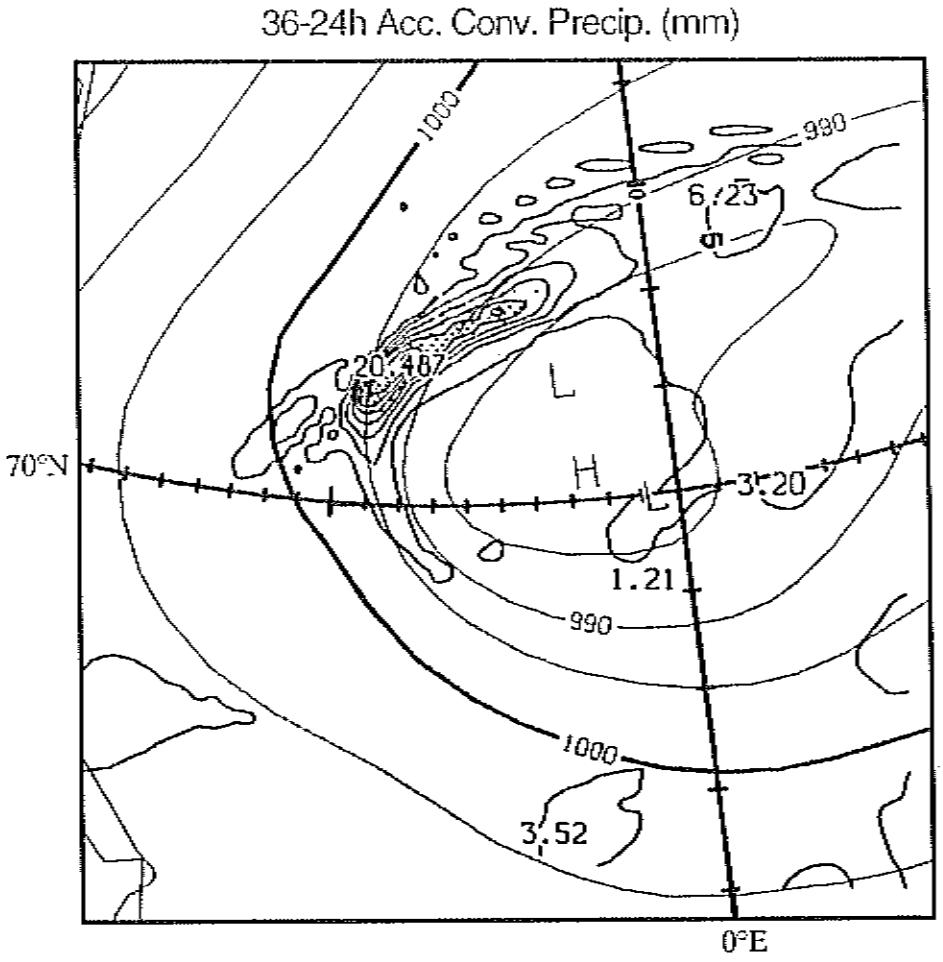

Fig.4 Simulated accumulated convective precipitation (mm) during 12 hours between T+24 and T+36h.

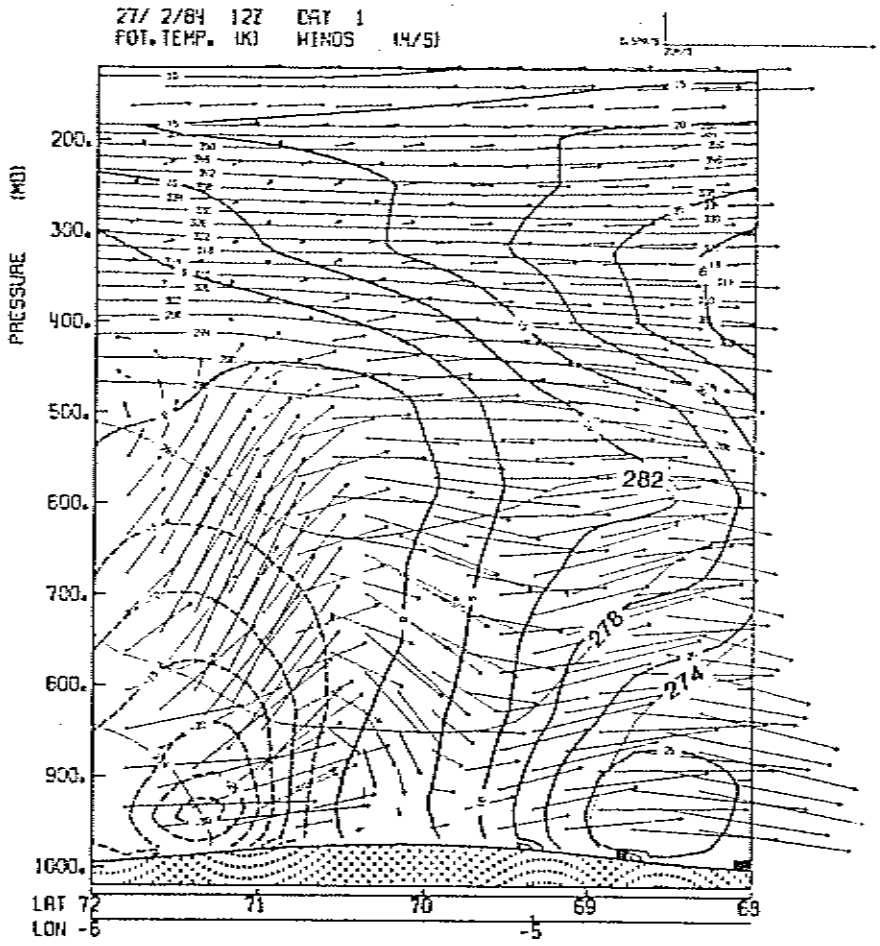

Fig.5 Cross-section along line AA' of Fig.1(b) of the simulated potential temperature (every 2K) and wind normal (isotachs) and parallel (arrows) to the cross section at T+36h.

model is not high enough for this case. However, the 274, 278 and 282 K contours of potential temperature can be seen at the same heights in both the cross sections. The vertical cross sections of the simulated omega and relative humidity fields are presented in Fig. 6. Although it is not possible to compare them with observations it is interesting to notice the realism of the vertical structures reproduced by the model. As in the actual polar low, the features represented are all confined in the part of the troposphere below 500 hPa. A cell of downward motion between two cells of upward motion represents the subsidence of dry air (Fig. 6b) corresponding to the eye of this cyclone. The maximum of vertical velocity, that was observed reaching peeks of 2 and 3 m/s, presents a maximum value of -2.4 hPa for the omega field produced by the model.

The model surface sensible and latent heat fluxes shown in Figs. 7a and b are of the same order of magnitude as observed (*SHF* 's Figs. 7c and d), although they are less intense and not so close to the centre of the cyclone as in reality, indicating again the limits of the resolution of the model. However, it is interesting to notice that, when simulating hurricanes like "Hugo" and "Gilbert" (not shown), the model is capable of producing surface latent heat fluxes one order of magnitude higher than surface sensible heat fluxes as observed (*SHF*).

To obtain an accurate forecast of a polar low it would be necessary to couple the atmospheric model with an ocean model capable of giving the sea surface temperature driven by the wind. As a matter of fact the well established effect of hurricanes on the sea surface temperature (*Black et al.*, 1989) was also observed for this polar low. Given the major importance of the surface sensible heat fluxes in a case of polar low, in a case of a hurricane it appears evident that there is a need for an accurate analysis and forecast of the sea surface temperature in order to accurately predict this phenomenon.

While observations of this kind are very useful in validating the simulation of a polar low, it is evident that they are costly and discontinuous. An ideal solution would be the remote sensing observation. A recent article from *Claude et al.*, 1992 shows how satellite observations can be used to detect a polar low and evaluate the relevant parameters. A combination of SSM/I, GEOSAT and TOVS observations are used to reach this goal and a comparison with results from the Norwegian LAM gives an idea of the possibility of this approach. Limitations due to the different resolution or operability of various instruments will be certainly overcome in the near future.

3. A MEDITERRANEAN STORM

In this section a description is given of the validation of results of a wave model (WAM) that uses, as input data, results from a simulation with the 40 km resolution LAM and a simulation with the ECMWF's global model at resolution T106. This is an indirect way of validating the simulation of the atmospheric models

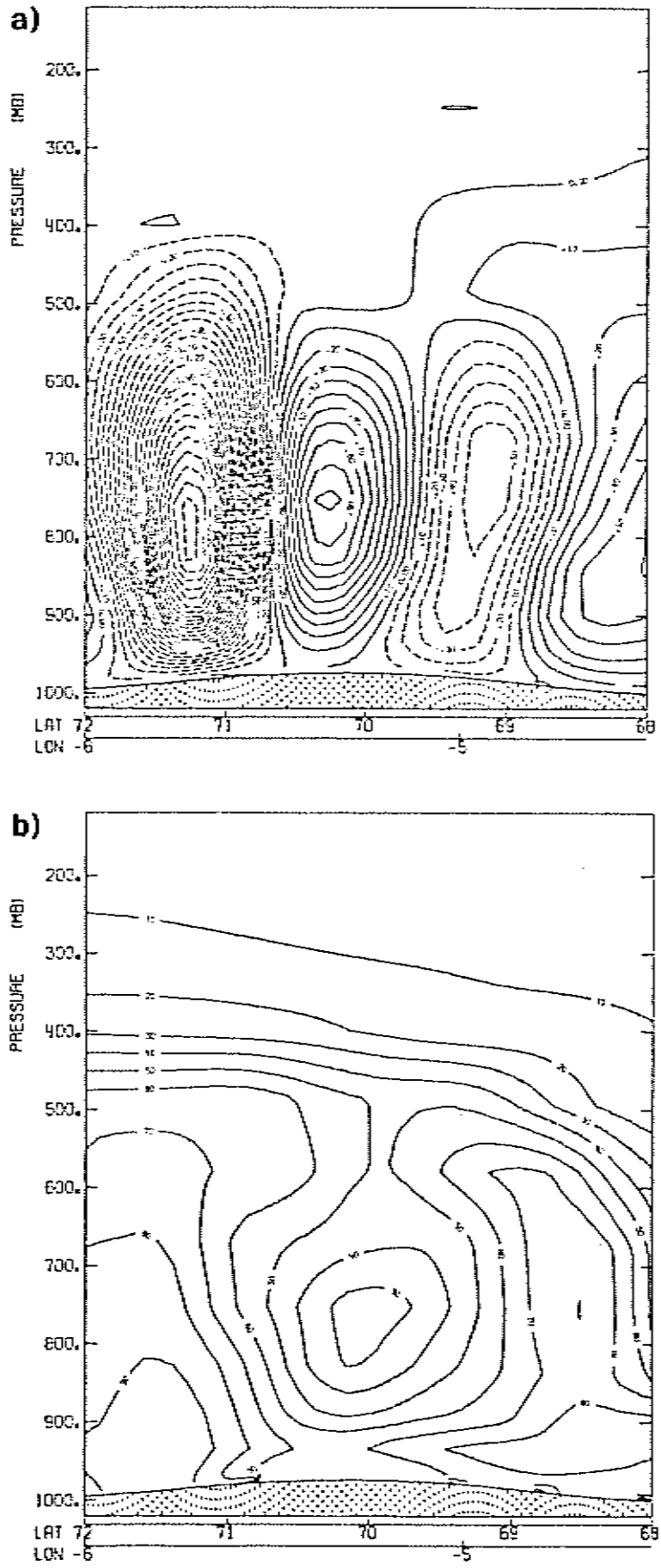

Fig.6 Cross-section along line AA' of Fig.1(b) of the simulated a) omega (Pa s^{-1}) and b) relative humidity (%).

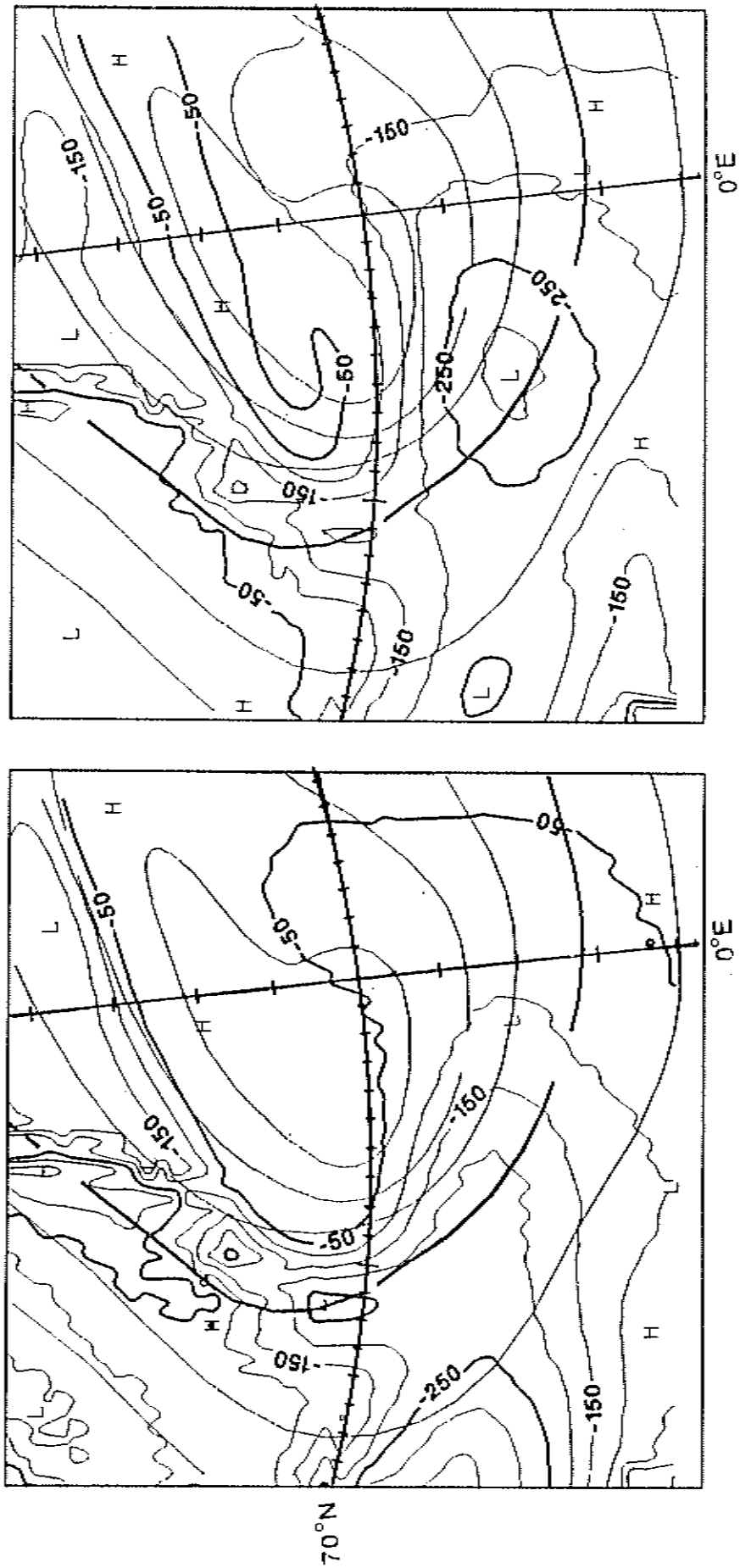

Fig.7 Simulated sensible (left) and latent (right) surface heat fluxes at T+36h.

that can give a measure of the importance of the correctness of their results. This kind of validation presumes that possible errors introduced by the wave model are small enough for the model to show clearly the effect of the atmospheric data.

On 2 December 1989, a violent storm over the central Mediterranean Sea in the region between Southern Italy and Malta disrupted the meeting between president Bush and president Gorbachov. Warmer subtropical air transported from the northern African region and cold air advected from northern Europe were the causes of the intense cyclogenesis that produced this so called "Gorbush" storm; a synoptic description of the event can be found in *Dell'Osso et al.*, 1992, hereafter *DBC*. Let us examine the result of the atmospheric and wave model starting from the latter. From Fig. 10 of *DBC* it appears that the LAM is able to capture the wave height at Crotone and with a certain delay at Catania (see *DBC*'s Fig. 1 for locations). The mean direction of the waves is almost acceptable at Catania but is on average 80 degrees out at Crotone. The global model, with a resolution three times lower, is less successful in predicting the wave height but more successful in predicting the wave direction. This appears more evident when comparing *DBC*'s Figs. 7 and 9 for the global and LAM wave height, and Figs. 6 and 8 for the global and LAM 10 m wind. It is evident that the global model is not capable of producing the right height of the wave because it is not capable of producing a sufficiently high wind speed. The LAM, however, intensifies the easterly and southeasterly wind reaching 20 m s^{-2} wind speed at Catania at 18 UTC 2 December (*DBC*'s Fig. 8), but is not able of reproducing the northwesterly flow along the coast of Southern Italy thus missing the wave direction at Crotone. At Malta the wave height estimated by the model with the LAM results (*DBC*'s Fig. 11) gives values consistent with the condition reported by local observers. The wave direction derived from the LAM, when compared with that measured (*DBC*'s Fig. 15), reflects an anticipation of the simulated wind in becoming southwesterly, and an overestimate of the wind speed after the veer. Comparing the analyzed with the LAM simulated MSLP (*DBC*'s Figs. 3f and 5d) it appears that the simulated low has been misplaced to the west of a distance that is important in the definition of the direction of the wind. However it is important to say that the wave direction is an integrated factor depending on the frequency of the waves not directly depending on the wind direction.

4. THE ATLANTIC CYCLONE

4.1 Synoptic description

The following description of the ERICA IOP4's cyclone that developed off the coasts of western United States during 4-5 January 1989, is based on/taken from the paper by *Neiman and Shapiro* (1992), *NS* hereafter. *NS* define this cyclone as a classic example of extreme extratropical oceanic cyclogenesis, that occurred during the cold season over an area of large sea-surface temperature gradients. The evolution of the cyclone described in *NS* is based on the unprecedented suite of in-situ and remote observing systems, deployed for the ERICA field programme.

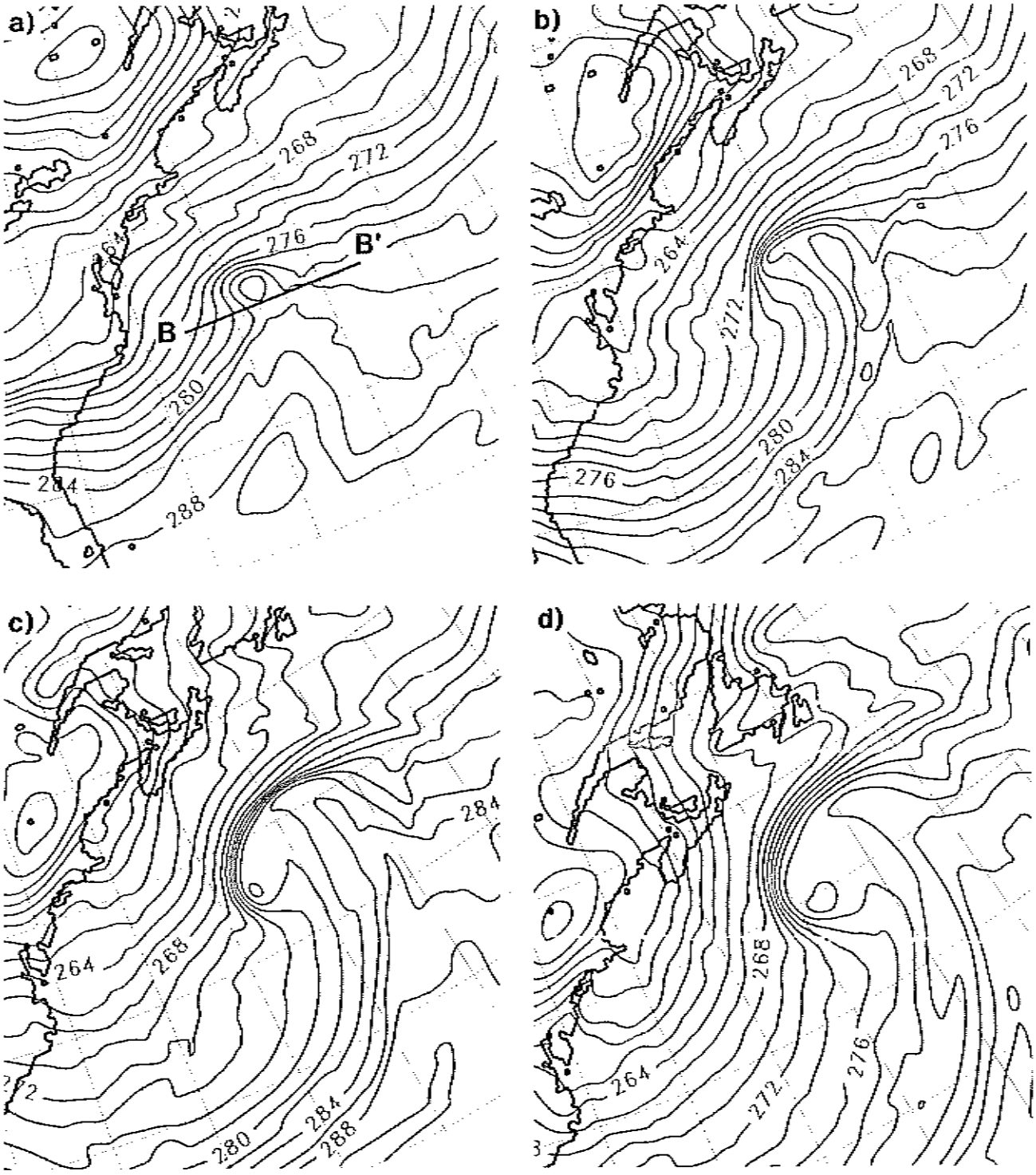

Fig.8 850 hPa simulated temperature (contours every 2K) at a) T+6, b) T+12, c) T+18, and d) T+24h, verifying respectively at 0600, 1200, 1800 UTC 4 January, and 0000 UTC 5 January, 1989.

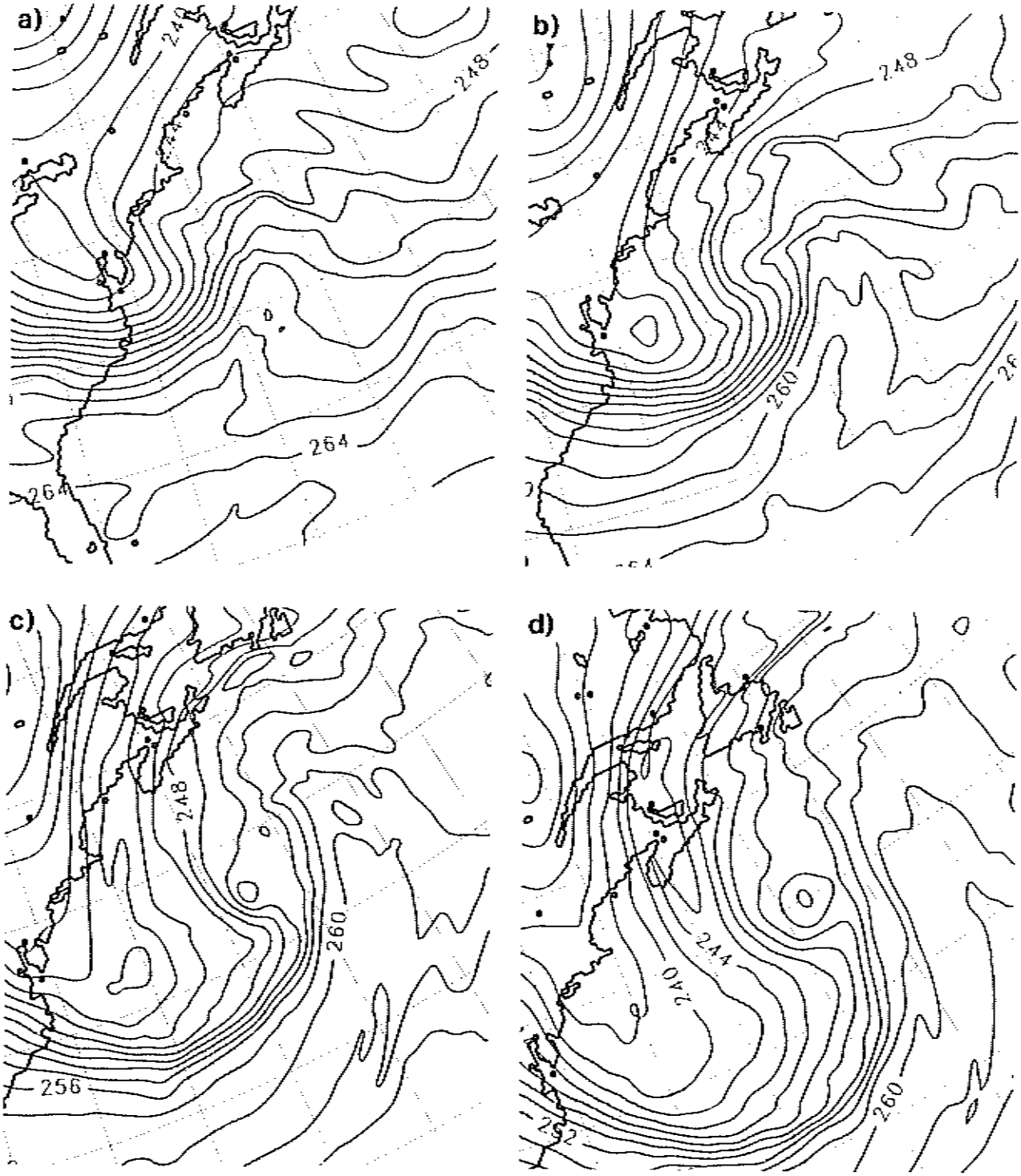

Fig.9 Same as Fig.8 for the 500 hPa temperature (contours every 2K).

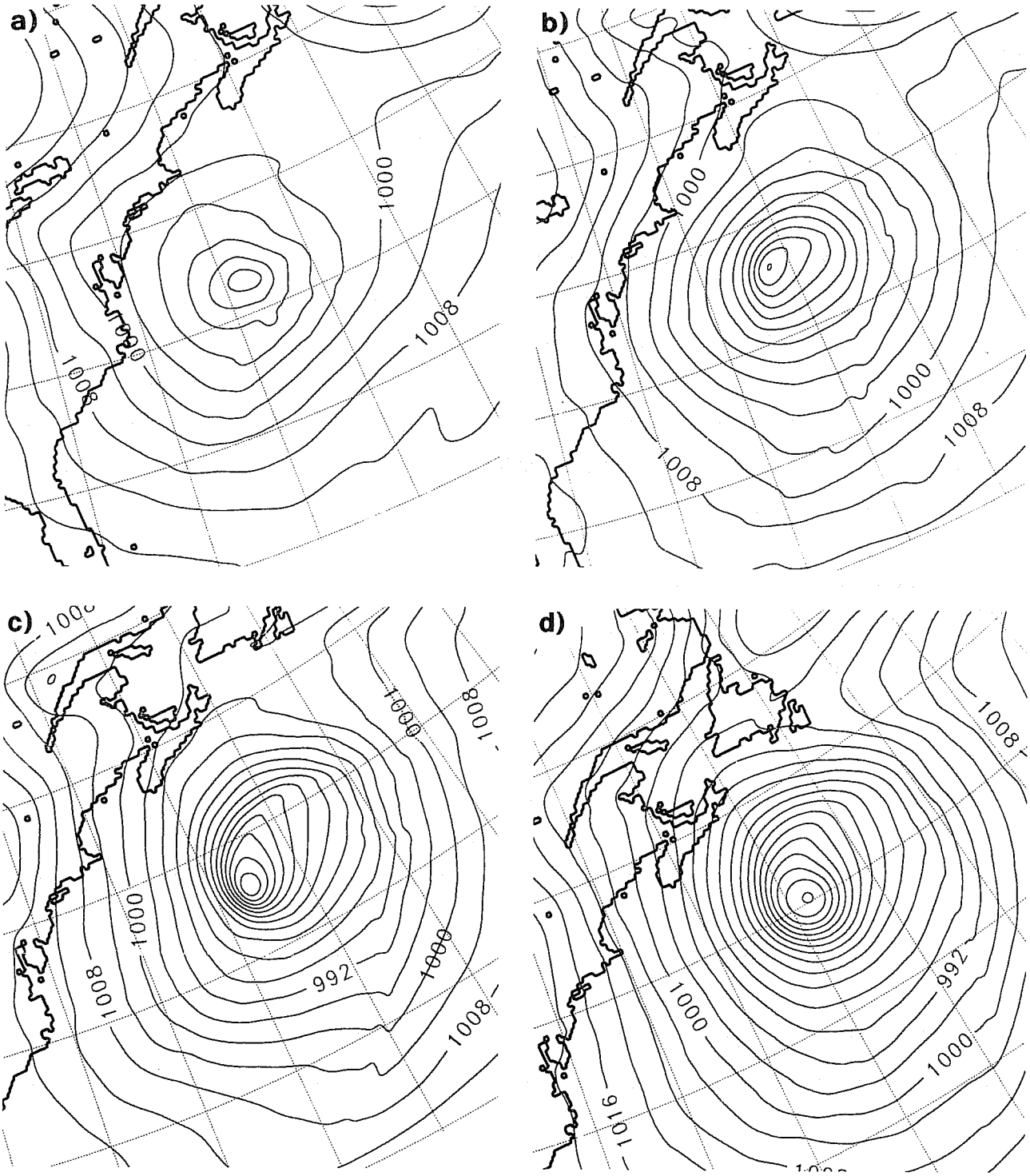

Fig.10 Same as Fig.8 for the mean sea level pressure (contours every 4 hPa).

At 0000 UTC 4 January 1989, a 500 hPa polar front advanced from the west towards a surface coastal trough and the incipient cyclone located over the warm Gulf Stream current east of 75° W. A region of upward motion at 700 hPa, ~ 22 m s^{-2} southwesterly surface wind over the warm ocean (20° C), and 1500 W m^{-2} sensible and latent heat fluxes characterize the initial stage of the cyclogenesis that commenced when the upper level jet-stream phased with the incipient cyclone, at the junction of the west-east oriented baroclinic zone and the southwest-northeast oriented coastal trough.

The analysis of the thermal evolution at 850 hPa shows a frontal contraction with the separation of cold and warm front at 0600 UTC. At 1200 UTC, warm and cold front reached the so called T-bone configuration. At 1800 UTC, the warm front bent back and extended southwestwards into the polar air stream, and a secondary front was created at the tip of it. This secondary front then dissipated in the next six hours. The seclusion of warmer air that already began at 1200 UTC reached its peak when the cold air of the secondary front encircled the warm pocket of previous post-cold-frontal air. At 0000 UTC, the warm air seclusion phase reached its maximum.

At 500 hPa the temperature analysis shows a weak baroclinicity at 0600 UTC. Then the warm baroclinicity increased and, by 1200 UTC, the bent-back and seclusion phase began. During the following hours the warm front weakened and became continuous with the cold front. The seclusion of warm air became quite large, and was vertically aligned with that at 850 hPa at 0000 UTC 5 January.

The cyclone central SLP went from 996 to 936 hPa in the 24-hour period between 0000 UTC 4 January and 0000 UTC 5 January. At 0600 UTC 4 January the cyclone centre was situated at the junction of the cold and warm front. Six hours later it migrated west of the junction, and, by 1800 UTC, it could be found almost 500 km from the junction. During the last 12 h, maximum wind speeds rotated cyclonically around the cyclone centre going from west to south-west and finally to the south of it. The centre of the surface cyclone was situated east of the 500 hPa centre at 0000 UTC 4 January, then it became vertically aligned with the 500 hPa front. During the last 12 hours the cyclone intensified beneath the warm core seclusion aloft. Cyclogenesis occurred on the cold side of the 500 hPa polar front and was decoupled from the upper level baroclinicity.

From the analysis of the sensible and latent heat fluxes it appears that upward fluxes of > 300 W m^{-2} sensible heat and > 1200 W m^{-2} latent heat were already present over the ocean into the warm sector of the incipient cyclone at 0000 UTC 4 January. The 20 m s^{-2} wind advecting colder air over the warm (> 20° C) Gulf Stream water was responsible for these heat fluxes that acted to reduce the static stability in the region of the cyclone. At 0600 UTC the maxima 400-500 W m^{-2} of sensible heat and 400-2600 W m^{-2} of latent heat fluxes could be seen north of the bent-back warm front and southwest of the cyclone centre,

respectively in the northerly and northwesterly flow. At 1200 UTC the sensible heat fluxes encircled the cyclone centre with maxima north (400 W m^{-2}), south-southwest (1000 W m^{-2}), and southeast (400 W m^{-2}) of it. The corresponding latent heat fluxes maxima were 1200, 2200, and 1600 W m^{-2}. Regions of 1000 W m^{-2} for the sensible heat and 1600 W m^{-2} for the latent heat fluxes could be found also near the coast where northwesterly cold air was advected over the warmer ocean. At 1800 UTC the 1800 W m^{-2} sensible heat flux maximum was situated in the northerly flow west of the bent-back front, and another maximum (500 W m^{-2}) could be seen in the warm region of the secondary front. Similar cyclonic rotation of the maxima could be found for the latent heat fluxes with 2800 W m^{-2} and 2400 W m^{-2}. Finally at 0000 UTC 5 January the maximum for the sensible heat (1200 W m^{-2}) and latent heat (3000 W m^{-2}) fluxes were located in the region south of the cyclone centre. At this stage, north and east of the cyclone centre the air being warmer than the ocean (< 10° C) the fluxes were directed downward.

4.2 MODEL RESULTS

Results of the simulation performed with the LAM at 20 km resolution will be compared with the observations analyzed in *NS*.

Figs. 8 and 9 describe the six-hourly evolution of the thermal front at 850 and 500 hPa respectively. They can be compared with the observation at the same time in *NS*'s Figs. 7 and 8. The simulated 850 hPa temperature field reproduce the phase of fracture of the thermal field (Fig. 8a) as well as the T-bone configuration (Fig. 8b) with the 10° C isoline describing the junction of the cold and warm font as in the observations. Fig. 8c shows the bending back of the warm front with strong gradient on the west side of the warm air seclusion (8° C). A secondary front at the tip of the bent-back front is also visible. At T+24 (Fig. 8d), the warm air in the secluded region is warmer (8° C) than observed (5° C). The secondary front does not encircle the warm seclusion with cold air entering it as observed. At 500 hPa the definition of the warm front is not clear as observed in the first 12 hours (Figs. 9a and b). Figs. 9c and d show a clear description of the region of warm air seclusion respectively at T+18 and T+24, and of the weakening of the warm front that becomes continuous with the cold front. The simulated region of warm air seclusion appears smaller than at 850 hPa, and warmer than observed, but, at T+24, it is vertically aligned with the 850 hPa seclusion as observed. Figs. 10 and 11, respectively describing the simulated SLP and the lowest model level wind, can be compared with *NS*'s Fig. 9. The central SLP simulated by the model goes from the analyzed 998 hPa at 0000 UTC 4 January to less than 940 hPa at 0000 UTC 5 January. A fall of pressure of more than 58 hPa in 24 hours, that is in good agreement with the observed 60 hPa. At T+6, T+12, and T+18 the simulated central pressure is 970, 960, and 945 against the observed 974, 960, and 941. From Fig. 10 it is possible to see the successive positions of the cold and warm front marked by the kinks in the isobars. The fronts are also clearly described by the wind field (Fig. 11) and by the 700 hPa field of vertical velocity (Fig. 12). As in the observation it is evident the migration towards west of the cyclone

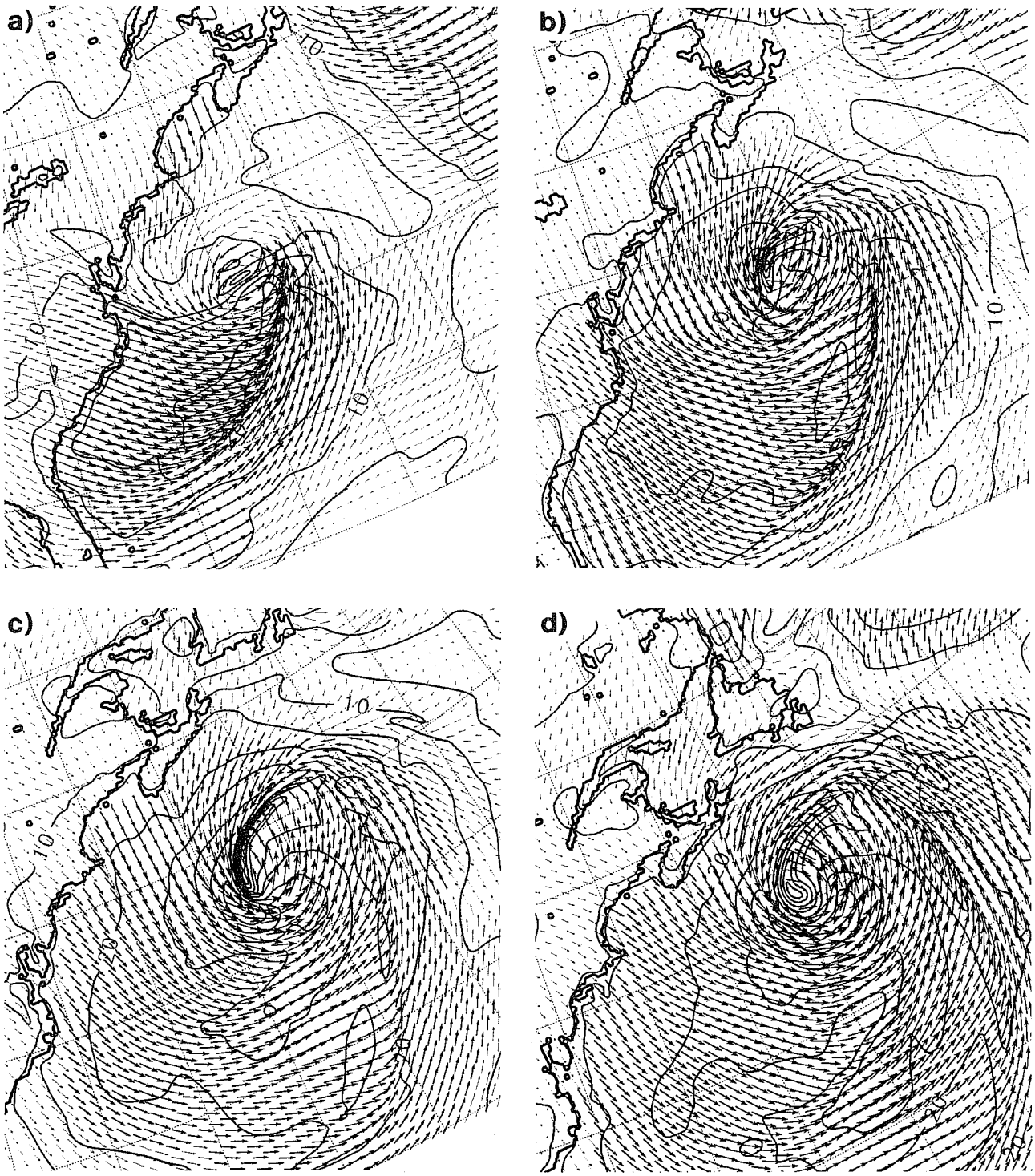

Fig.11 Same as Fig.8 for the wind (isotachs every 5ms^{-1}).

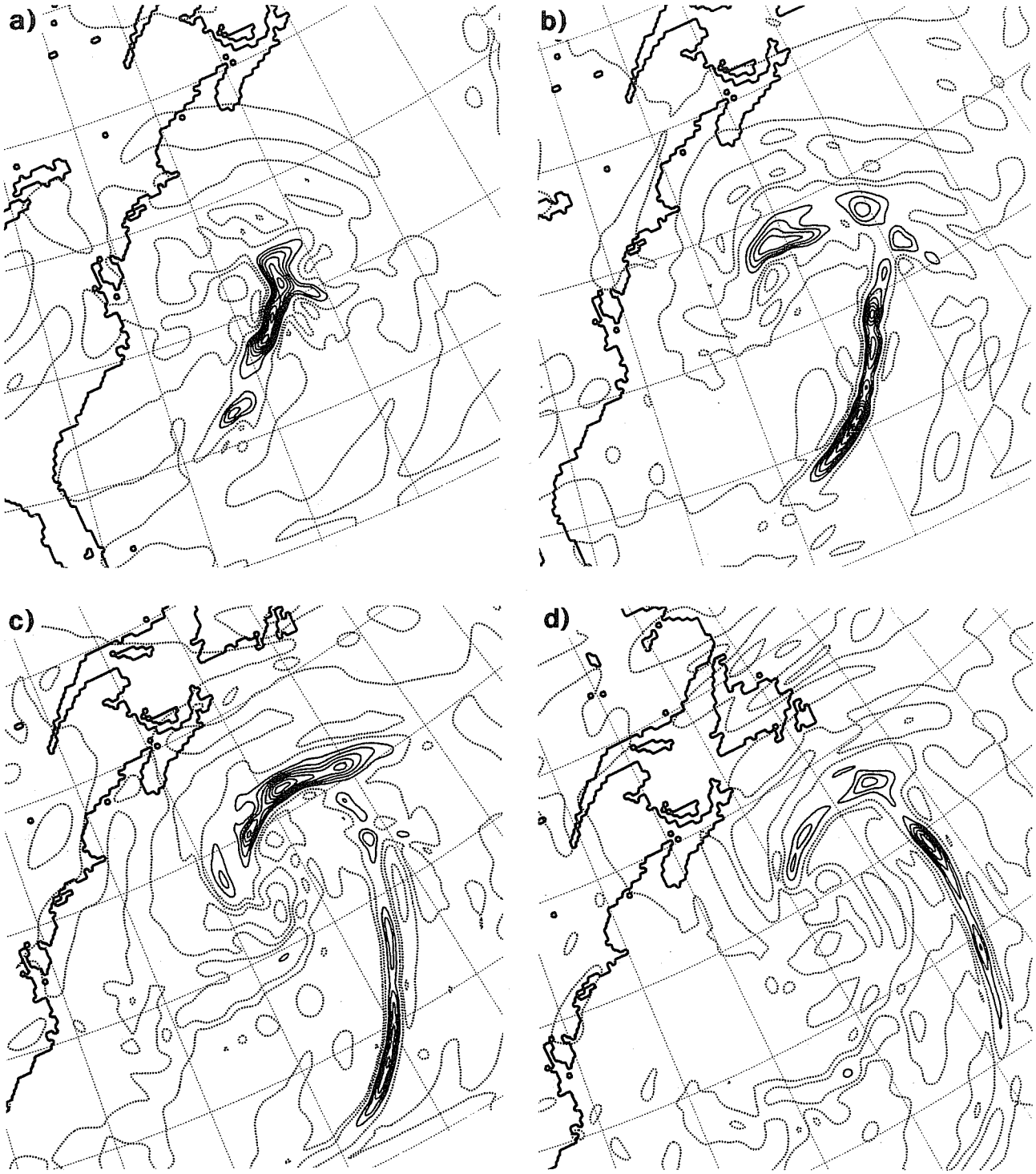

Fig.12 Same as Fig.8 for - omega at 700 hPa (contours every 0.8 Pa s^{-1}).

centre with respect to the junction between cold and warm front, as well as the increase of the SLP gradient and its cyclonic rotation around the cyclone centre. The vertical velocity field gives also a clear indication of the relative position of cold and warm front in their T-bone configuration stage and, at T+18 (Fig. 12c), also shows the secondary front at the southern tip of the bent-back warm front. As already seen this front does not encircle the pocket of warm air so tightly as observed, but it dissipates between T+18 and T+24 as observed. The wind speed that reaches a maximum of almost 45 m s^{-2} at T+18 decreases to 38 m s^{-2} at T+24, which is not the case for the observed wind that increased to a maximum 45 m s^{-2} at 0000 UTC 5 January. Figs. 13 and 14 show the evolution of the sensible and latent heat fluxes, which should be compared with the analogously observed fields in *NS*' Figs. 18 and 19. It should be taken into consideration that the observed fluxes are computed from data taken within + 2-3 hours surrounding a designed analysis time, while the fluxes from the model are averaged over the previous 6 hours. Therefore, when considering the wind that determines the fluxes, the direction and strength of the wind during the previous 6 hours must be taken into account. In the first 12 hours of simulation the cold continental northwesterly flow over the warm water off the coast around 35 N, and the northerly flow west of the bent-back warm front generate two maxima of sensible heat fluxes (respectively 550 and 350 W m^{-2}) and two maxima of latent heat fluxes (respectively 1400 and 600 W m^{-2}). At T+18 the sensible heat flux maximum off the coast is increased to 550 W m^{-2}, and the other maximum west of the bent-back front is 800 W m^{-2} and extends towards the south. The latent heat fluxes still show the effect of the previous six hours cold air flow with a 1300 W m^{-2} maximum, but now the absolute maximum is encircling the cyclone centre with 1450 W m^{-2} on the south of it. At T+24 the maximum sensible heat (880 W m^{-2}) is still on the southwest side of the cyclone centre and high values extend towards the east. Negative values of sensible heat fluxes appear over the eastern region east of the T+12 cold front. The temperature of the ocean is here colder than the air temperature and the fluxes reverse their direction. At this time a maximum of more than 1700 W m^{-2} of latent heat fluxes is situated south of the cyclone centre. Other secondary maxima can be seen in both fields west of the polar front, *NS* explain them as the effect of a downward intrusion of post-frontal dry air from aloft (Figs. 12b and c). The simulated maximum of sensible and latent heat fluxes higher than 2600 W m^{-2} to be compared with the observed more than 4000 W m^{-2} demonstrate that the model is capable of reproducing this high value of fluxes that are characteristic of this extreme case of cyclone, but, on the other hand, it also shows the limits of the model itself.

Let us now compare the results from the model simulation with the more detailed analysis of the cyclone from *Neiman et al.*, 1992, hereafter *NSFG*. In their Fig. 3 the area to be studied in more detail is shown for 0600, 1800 UTC 4 January, and for 0000 UTC 5 January. A mesoscale analysis of the enlarged area at 0600 UTC shows the presence of three small scale lows (*NSFG*'s Fig. 5) in the region of contraction of the thermal field, one of them will evolve into the major low. Nothing of this kind can be seen by enlarging the equivalent area of the model results. The cross section of the simulated potential temperature and

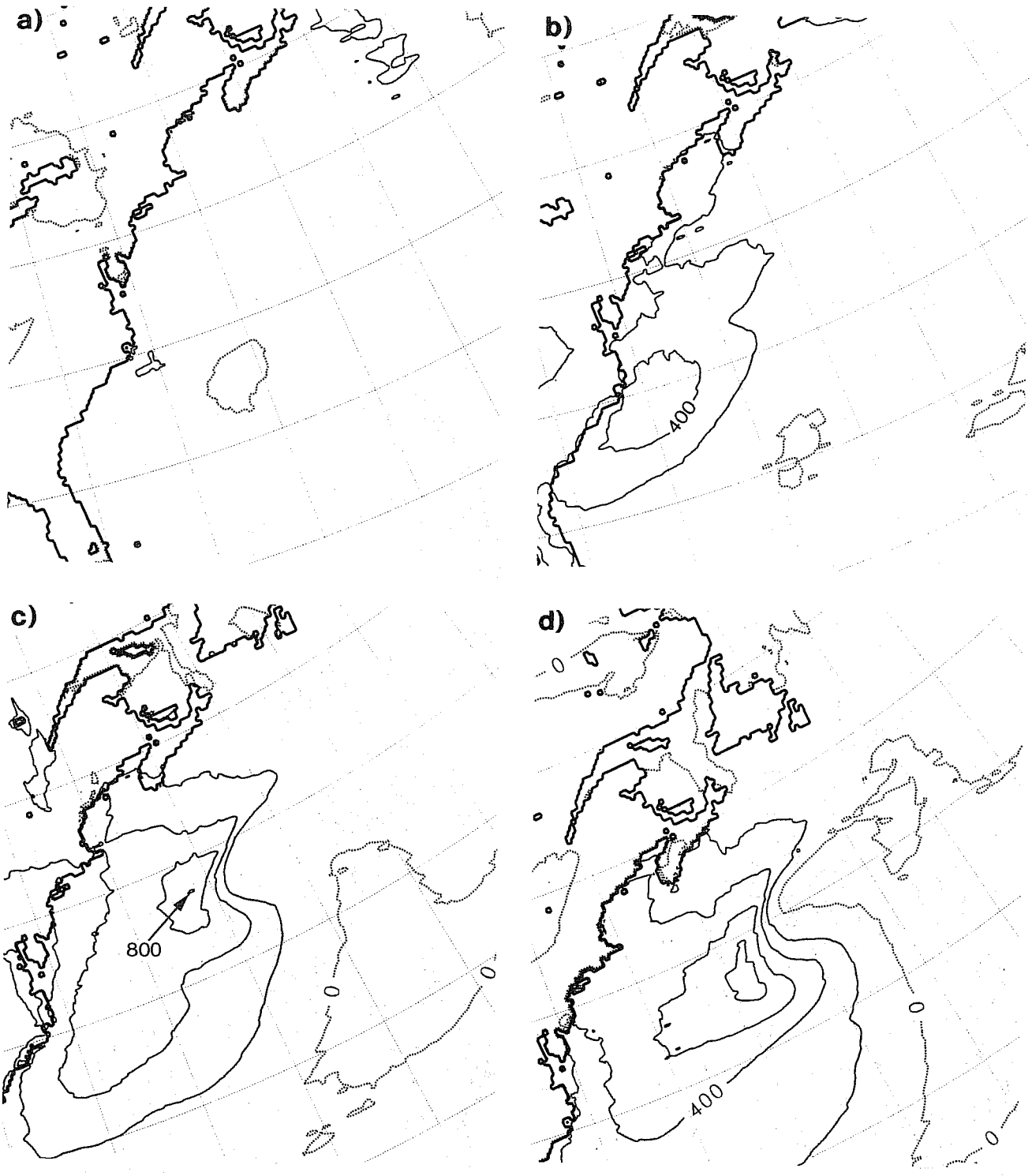

Fig.13 Same as Fig.8 for surface sensible heat fluxes (contours every 200 W m^{-2}).

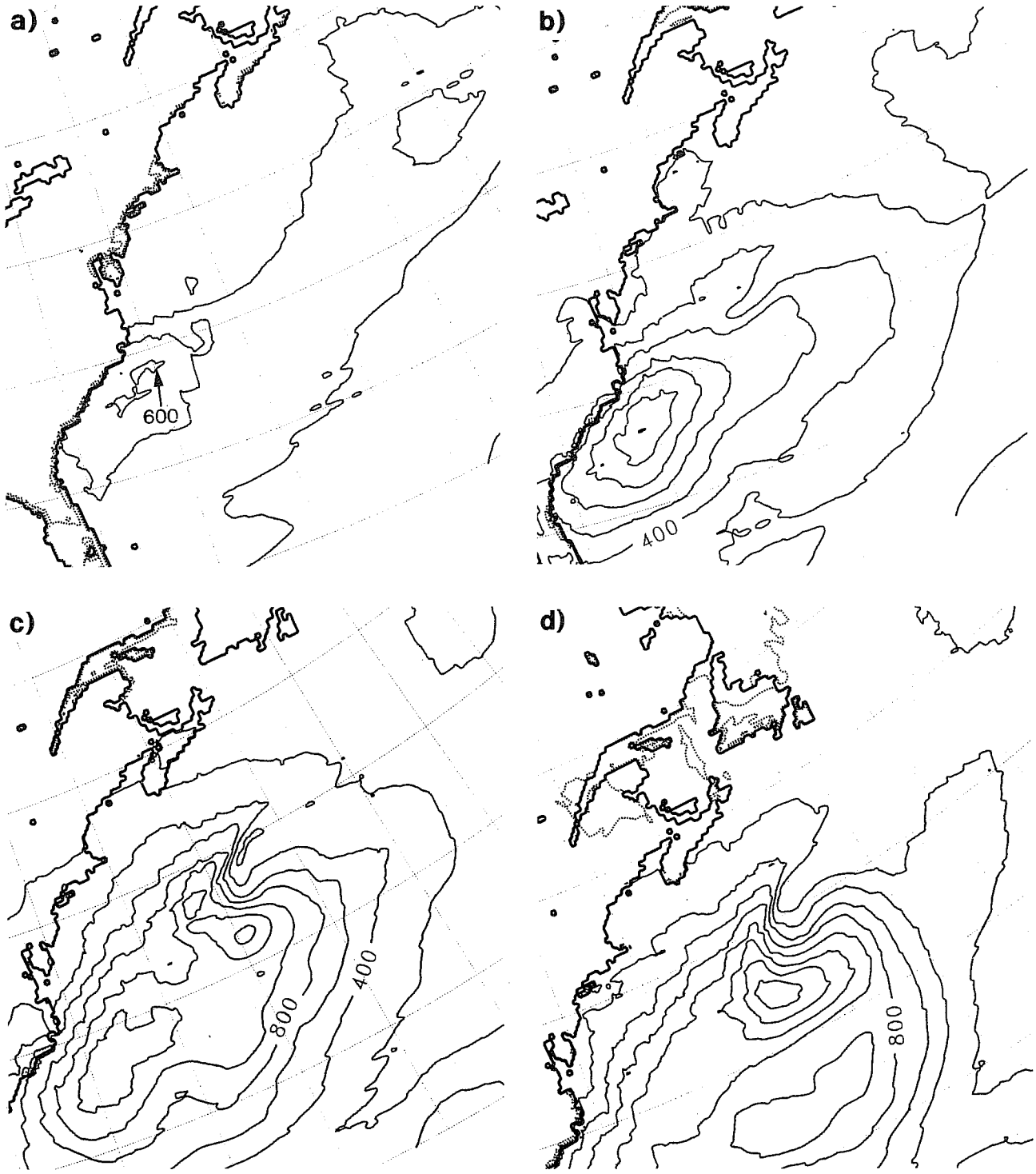

Fig.14 Same as Fig.13 for the latent heat fluxes.

section-normal wind velocity (Fig. 15) along the line BB' of Fig. 8a, to be compared with *NSFG*'s Fig. 9, shows the cold front extending upward and sloping eastward, that is in the opposite direction from the observed, with northerly wind (coming out from the cross-section) confined below 600 hPa, as in *NSFG*'s. The column of vertical velocity ahead of the leading edge of the cold front with a maximum of more than 7 hPa s^{-2} above 600 hPa can be validated by the deep (8-20 km) cumulus convective clouds observed east of the polar front. High values of vertical velocity were reported by the 350 m above level ground flight with instantaneous maxima of 7 m s^{-2}. The so called T-bone/incipient warm core seclusion at 1800 UTC 4 January is the other phase of the cyclone analyzed in great detail by *NSFG*. Their Fig. 13a, representing the 350 m equivalent potential temperature analysis can be compared rather well with that simulated (Fig. 16) at 900 hPa (at this stage, the simulated centre pressure is 945 hPa). The > 314 K incipient warm seclusion is represented by a closed 316 K contour, and the 322-326 K intrusion paralleling the cold front is represented by a 322 K isoline. The streamlines at 900 hPa (Fig. 17b) are very similar to that observed at 350 m (*NSFG*'s Fig. 13b), with a confluent asymptote extending along the warm front, another situated at the polar cold front, another confluent asymptote at the edge of the secondary cold front, and possibly a third confluent asymptote at the leading edge of the secondary front. At 400 hPa the centre of the outflow (Fig. 17a) is situated at 300 km from the 900 hPa cyclone centre, double of the observed (*NSFG*'s Fig. 14). As in the observation the vertical structure of the simulated storm circulation shows cyclonic inflow at lower troposphere and cyclonic outflow in the middle troposphere. The outflow from the cyclone centre spirales northward and westward toward a col-point as in the observations, and southeastward and eastward in a confluent flow that was also observed. The potential temperature and wind cross-section through the bent-back front along line EE' (Fig. 18) is similar to the equivalent cross-section in *NSFG*'s Fig. 17. The front extends upward and northwestward, broadening with height. A low level jet of 40 m s^{-2} is situated in the northwesterly flow beneath the front as observed. Finally the enlarged figure of the secluded warm air at 0000 UTC 5 February (*NSFG*'s Fig. 19a) is represented by the simulated equivalent potential temperature field of Fig. 19. Here, two close contours with maximum θ > 318 K represents a remarkable success in reproducing this warm seclusion area, where a 322 K close contour was observed only in a small region with a diameter of about 20 km. The potential temperature and wind cross-section along the line GG' of Fig. 19 (Fig. 20), to be compared with *NSFG*'s Fig. 22, shows that the simulated warm core seclusion is not as shallow as observed. The maximum wind speed are found in the marine boundary layer with 30 and 50 m s^{-2}, but, as already said, the simulation is not capable of reproducing the large gradient east of the cyclone centre.

5. CONCLUSIONS

The validation of experiments performed with high resolution numerical models is often problematic. A numerical model produces a very dense and regularly spaced set of results, while observations are scarce in space and time. Furthermore, in some cases, the hand drawn analysis of the observations is made with

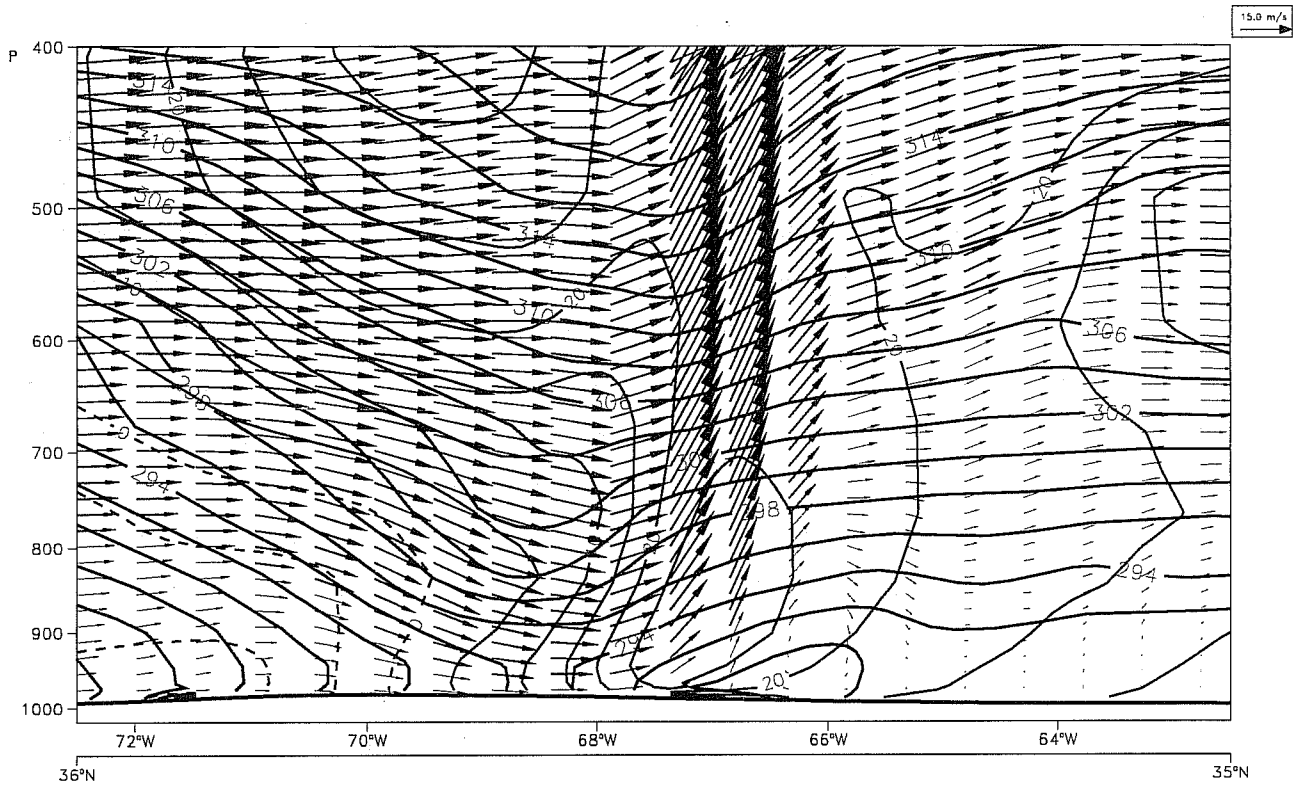

Fig.15 Cross-section along line BB' of Fig.8(a) of the simulated potential temperature and wind normal (isotachs every 5 ms^{-1}) and parallel (arrows) to the cross-section.

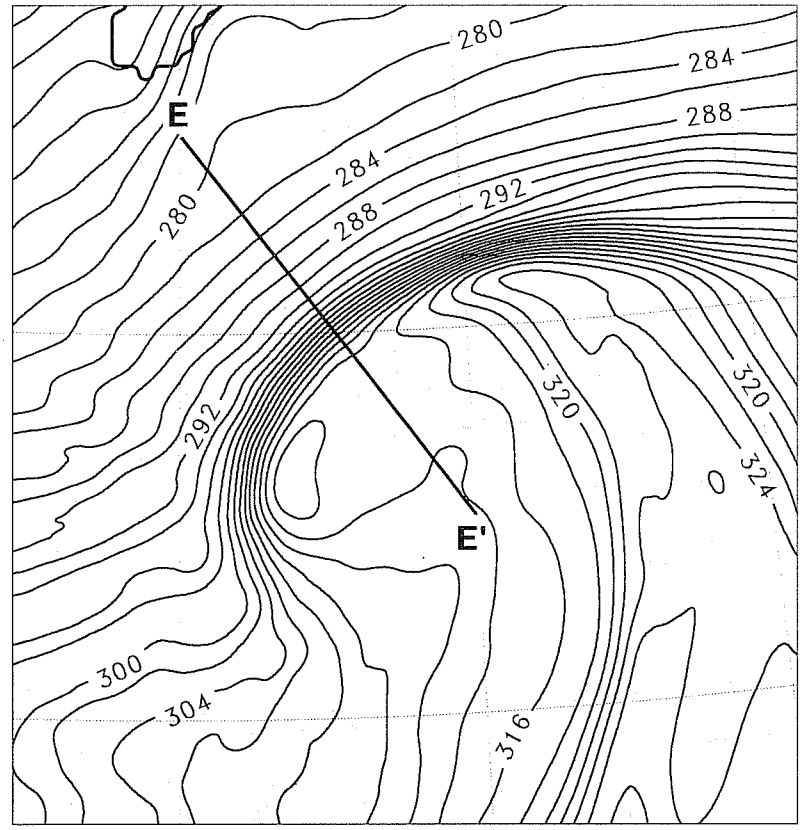

Fig.16 Simulated 900 hPa equivalent potential temperature (contours every 2K) at T+18h.

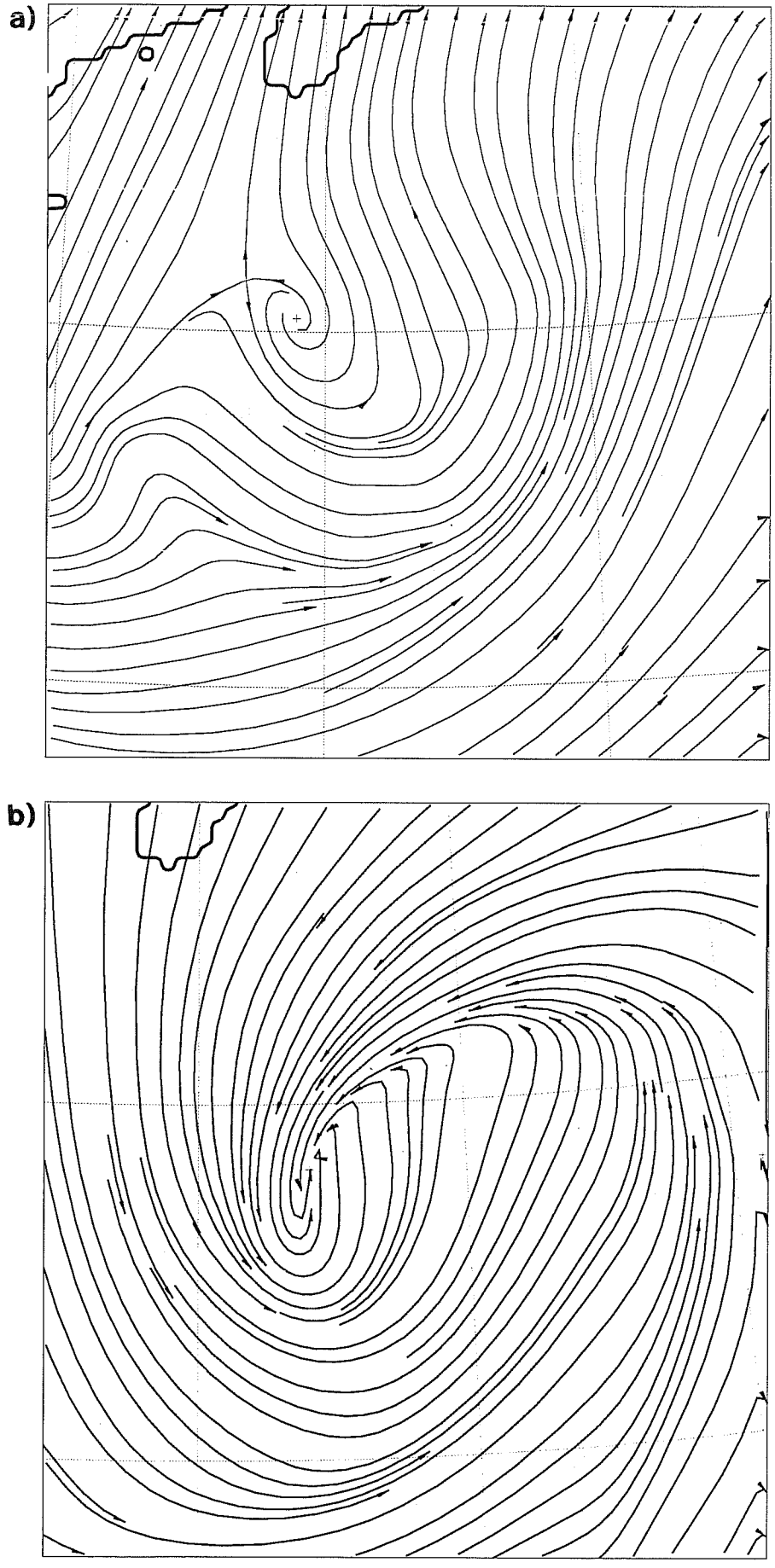

Fig.17 Simulated streamlines at a) 400 hPa, and b) 900 hPa at T+18h.

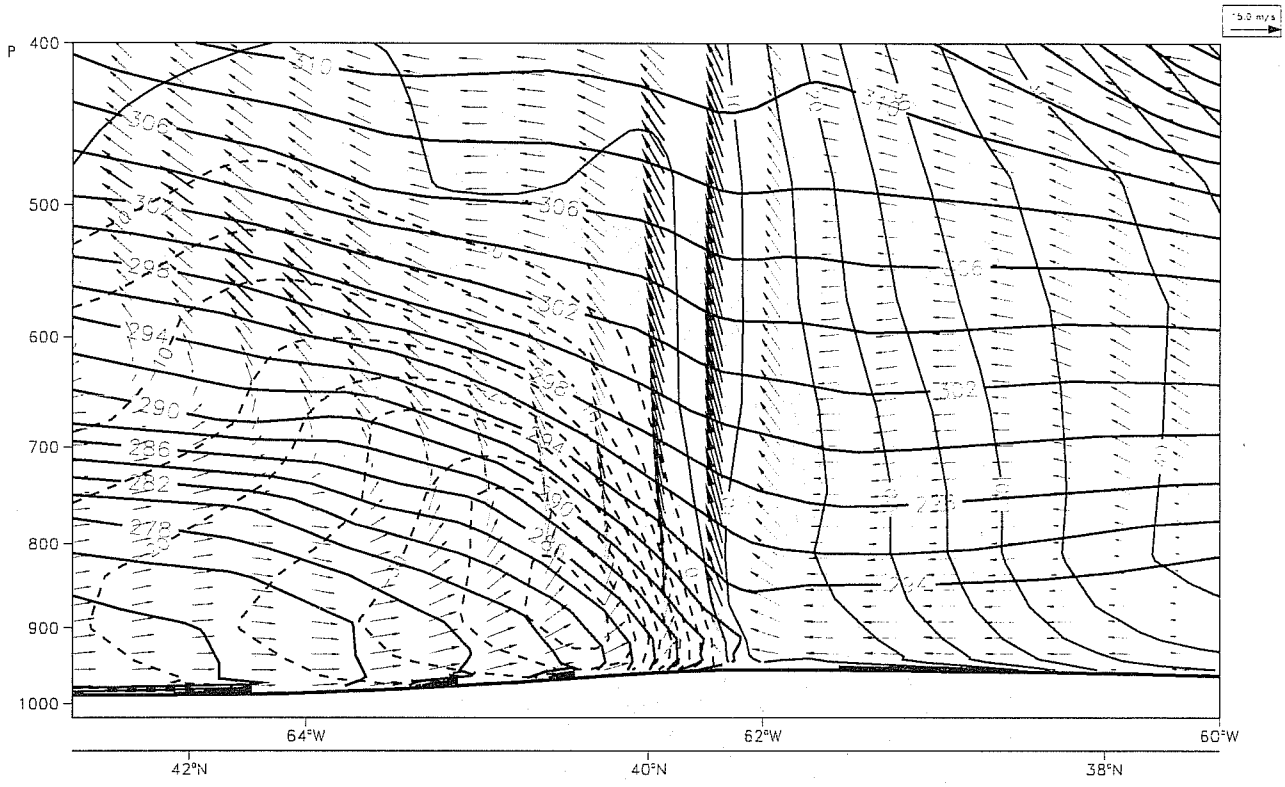

Fig.18 Cross-section along line EE' of Fig.16 of the simulated potential temperature and wind normal (isotachs every 5 ms^{-1}) and parallel (arrows) to the cross-section.

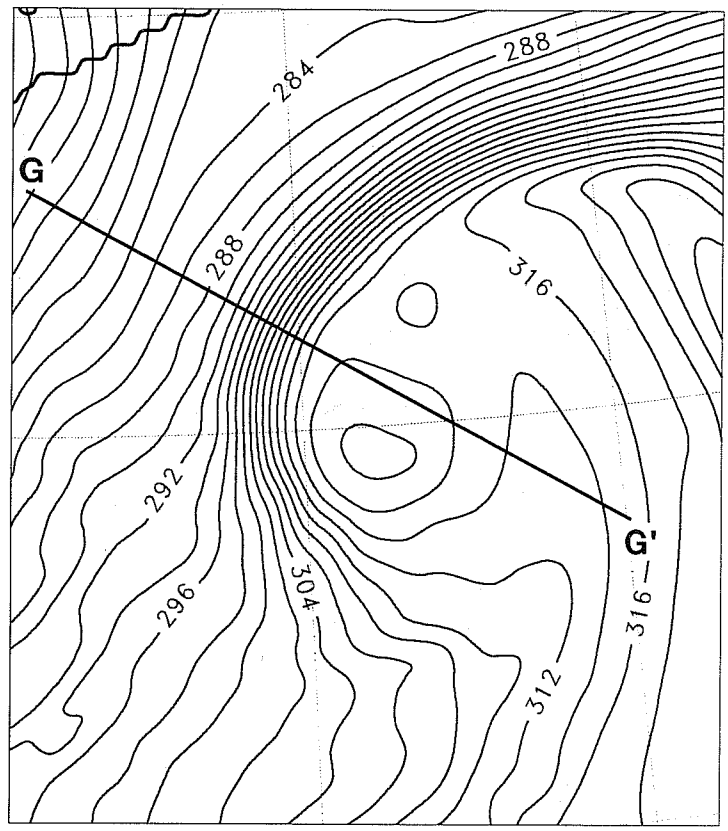

Fig.19 Same as Fig.16 at T+24h.

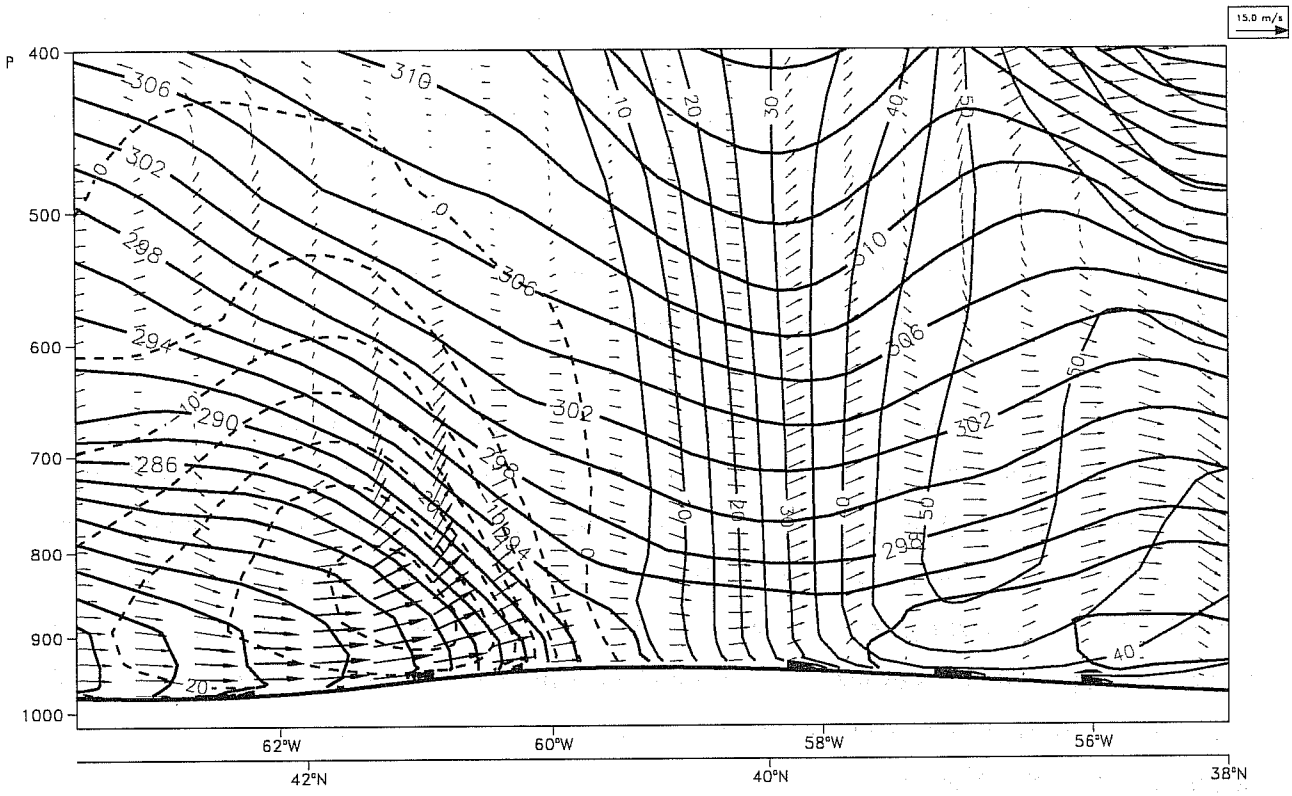

Fig.20 Cross-section (as in Fig.15) along line GG' of Fig.19.

the help of numerical model results to interpret data or to interpolate or extrapolate them. Despite this, observations from field experiments are the most useful source of data for comparison and validation of model results. In this article data obtained in a case of polar low could be compared with the simulation from a 20 km horizontal resolution limited area model. From this comparison it can be said that the model is capable of reproducing the vertical structure of the polar low as well as reproducing wind maxima, sea level pressure and surface fluxes of the same order of magnitude as observed. On the other hand it is evident that 20 km is the upper limit of a grid size to simulate this phenomenon. The area covered by the simulated low was, in fact, much broader than observed.

The model, at 20 km horizontal resolution, gave also a good representation of the ERICA storm of the 4 January 1989. Details of the evolution of the vertical structure of the cyclone, its thermal field, wind speed, surface pressure and surface fluxes were well reproduced by the model. The physics of the model proved to be capable of going from low to high resolution without need of tuning. However, when comparing the very fine structure of the pressure field at the initial stage of the evolution of the cyclone, the limitation of the model is evident. The fine multiple structure of the depression that later on evolved in a single explosive cyclone could not be reproduced by the model with a resolution lower than this particular scale of the phenomenon.

REFERENCES

Claude, C., N.M. Mognard, K. Katrsaros, A. Chedin, and N. Scott, 1992: Satellite Observations of a Polar Low over the Norwegian Sea by SSM/I, Geosat and TOVS. Submitted to Jour.Geoph.Res.

Black, P.G., L.K. Shay, R.L. Elsberry and J.D. Hawkins, 1989: Response of the Gulf of Mexico to Hurricane Gilbert. 18th Conference on hurricanes and tropical meteorology. Am.Met.Soc., San Diego, Calif., 15C, 4.

Dell'Osso, L., L. Bertotti and L. Cavaleri, 1992: The Gorbush storm in the Mediterranean Sea: Atmspheric and Wave Simulation. Mon.Wea.Rev., 120, 77-90.

Neiman, P.J., and M.A. Shapiro, 1992: The Life Cycle of an Extratropical Marine Cyclone. Part I: Frontal-Cyclone Evolution and Thermodynamic Air-Sea Interaction. Submitted to Mon.Wea.Rev.

Neiman, P.J., M.A. Shapiro, L.S. Fedor, and F. Gonzalez, 1992: The Life Cycle of an Extratropical Marine Cyclone. Part II: Mesoscale Structure and Diagnostics. Submitted to Mon.Wea.Rev.

Reed, R.J., 1988: Polar lows. ECMWF Seminar Proceedings 1987, vol 1, 213-236.

Shapiro, M., L.S. Fedor and T. Hampel, 1987: Research aircraft measurements of a polar low over the Norwegian Sea. Tellus, 39A, 272-306.